

# Dynamic Correlation between Pressure-Induced Protein Structural Transition and Water Penetration

Takashi Imai<sup>\*,†</sup> and Yuji Sugita<sup>‡</sup>

Computational Science Research Program and Advanced Science Institute, RIKEN, Wako,  
Saitama 351-0112, Japan

Received: October 10, 2009; Revised Manuscript Received: January 12, 2010

Water penetration into the hydrophobic interior of proteins has been postulated to be a primary force driving pressure-induced denaturation of proteins. The water penetration model is supported by several theoretical and simulation studies, although its direct evidence is lacking. In this study, 1  $\mu$ s all-atom molecular dynamics simulations of ubiquitin in explicit water at high and low pressures are performed to examine the water penetration model. The high-pressure simulation starts from a crystal structure at atmospheric pressure and successfully reproduces the main characteristics of a high-pressure structure obtained by NMR. Water penetrates into a specific hydrophobic core of the protein and is ejected from the interior several times. The structural transition results from the relative stabilization of a preexisting metastable structure by applying pressure. A time correlation analysis demonstrates that the transition is accompanied by the penetration of water within a time scale comparable to the relaxation time of water itself. Simultaneous water penetration only occurs above a certain high pressure.

## Introduction

Pressure-induced denaturation or structural transition of proteins continues to attract attention as one of the outstanding properties of proteins,<sup>1–4</sup> ever since Bridgman<sup>5</sup> observed it as coagulation of egg white under a hydrostatic pressure of several thousand bar. In addition to scientific interest, the pressure effect is important in industrial applications, particularly in the food-processing industry.<sup>6</sup>

Although several hypothetical models have been proposed to explain the pressure denaturation, the molecular mechanism has still not been completely elucidated. Nevertheless, most researchers currently consider that the primary driving force for pressure denaturation is the penetration of water molecules into the protein interior. The water penetration model was proposed in a pioneer theoretical study by Hummer et al.,<sup>7</sup> who demonstrated that high pressure increases the stability of water-mediated contact between two methane molecules in water relative to direct contact. This result implies a possible mechanism in which high pressure squeezes water molecules into the hydrophobic core of a protein, resulting in swelling of the protein.

In the past several years, the significance of water penetration has been repeatedly emphasized by several molecular dynamics (MD) simulation studies. Paliwal et al.<sup>8</sup> used a trick to reproduce the pressure-induced unfolding of staphylococcal nuclease in their nanosecond-scale MD simulation, since pressure denaturation is a much slower process than could be simulated with the computing capabilities of that time. They randomly inserted water molecules into the protein interior in MD simulations at progressively higher pressures to drive the protein to unfold efficiently. The structure so obtained was consistent with a two-domain structure derived from the small-angle neutron scattering

pattern under high pressure. Another approach was adopted by Collins et al.,<sup>9</sup> who examined water filling in a hydrophobic cavity created by mutation in T4 lysozyme under high pressure. They performed nanosecond-scale MD simulations under different initial conditions in which 0–5 water molecules were artificially located in the cavity, at different pressures. The calculations indicated a transition from a predominantly empty cavity at atmospheric pressure to a cavity filled by approximately four water molecules at 2000 bar, even though the protein structure itself was not significantly changed. Day and García<sup>10</sup> conducted nanosecond-scale MD simulations of ubiquitin at low and high pressures, starting from low and high-pressure structures (LPS and HPS, respectively) determined by NMR measurement. They found that the number of penetrating water molecules in HPS under high pressure is about 5 more than that in LPS under low pressure, though a structural transition was not observed in the simulations.

The water penetration model has also been supported by recent studies based on the integral equation theory of liquids. Harano and Kinoshita<sup>11</sup> investigated the pressure dependence of the solvation free energies for several different structures of protein G, including native, partially unfolded, and random coil structures, using the three-dimensional (3D) integral equation theory for a hard-body model. They found that only the swelling structure that allows solvent penetration is stabilized at elevated pressures relative to the native structure. Imai et al.<sup>12</sup> calculated the difference in the partial molar volume (PMV) between the LPS and HPS of ubiquitin using the 3D reference interaction site model (RISM) theory and demonstrated that the pressure-induced structural transition reduces the PMV, implying that HPS can be stabilized relatively at increased pressures through a law of thermodynamics known as Le Chatelier's principle. Further analysis indicated that the PMV reduction is attributed to the penetration of water into a specific cavity created by the structural transition.

Although these computational studies provide evidence for the significance of water penetration in pressure denaturation

\* To whom correspondence should be addressed. E-mail: takashi.imai@riken.jp.

<sup>†</sup> Computational Science Research Program.

<sup>‡</sup> Advanced Science Institute.

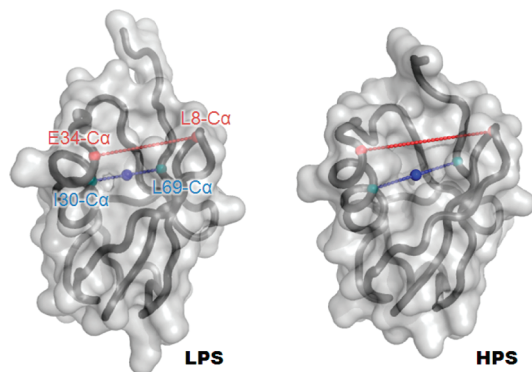


**Figure 1.** Low and high-pressure structures of ubiquitin in aqueous solution determined by NMR. Shown are the transparent surface and tube representations of the averaged structures of each 10 structures deposited in PDB (1v80 for LPS and 1v81 for HPS). The atoms colored red and blue are used to monitor the local structure and the cavity center, respectively (See text).

of proteins, the following two important issues still remain to be resolved. First, the structural transitions occurring under high pressure have never been observed in MD simulations without artificial water insertions. Second, the dynamic correlation between protein structural transitions and water penetration has not been clarified. There are some dynamically different pictures for water penetration, which cannot be distinguished by the previous studies. Do water molecules first penetrate into the protein interior forcing the protein to swell or are cavities first induced by intrinsic structural fluctuations followed by water entry?

In this study, we performed 1  $\mu$ s MD simulations, which are longer than the previous simulations almost by 2 orders of magnitude, at high as well as low pressures, starting from a single X-ray crystal structure, in order to examine the relationship between any protein structural transition and possible water penetration. We chose again ubiquitin as the target protein because it is one of few proteins whose HPSs in solution are known in atomic resolution. The HPS at 3000 bar resolved by NMR<sup>13</sup> is shown in Figure 1, along with the LPS at 30 bar. The most significant difference in structure is found in the central cleft: It is open in HPS and closed in LPS. For our study, local-structure transitions are more pertinent than global unfolding since partial denaturation can be expected to occur within a time scale of microsecond, whereas complete denaturation as observed under much higher pressure<sup>14</sup> would not be seen even in a microsecond-scale simulation.

We clarify in this paper the differences in protein structure and the behavior of water molecules around the protein depending on the pressure, based on the 1  $\mu$ s MD simulations of ubiquitin at three pressures of 1, 3000, and 6000 bar. We then discuss the dynamic correlation between the protein structural change and the water penetration under high pressure in relation to the water penetration model proposed earlier.

## Computational Methods

MD simulations of ubiquitin in explicit water were performed with the double precision compiled version of GROMACS 4.0<sup>15</sup> and Amber99SB force field<sup>16</sup> ported into GROMACS.<sup>17</sup> The initial structure (PDB code 1UBQ<sup>18</sup>) was solvated by 12 023 SPC/E<sup>19</sup> water molecules in a  $72 \times 72 \times 72 \text{ \AA}^3$  rectangular box. No ions were added because ubiquitin is neutral. After energy minimization, a 200 ps NVT MD simulation was performed for equilibration at 298.15 K, followed by 200 ps

NPT equilibration runs at 298.15 K and the target pressures (1, 3000, and 6000 bar). Temperature and pressure were controlled using the weak coupling scheme of Berendsen<sup>20</sup> in these preliminary equilibration runs. Then, another 200 ps NPT equilibration using Nosé–Hoover thermostat<sup>21,22</sup> and Parrinello–Rahman barostat<sup>23,24</sup> was implemented for each pressure in the run-up to the production run of 1  $\mu$ s duration. Long-range electrostatic interactions were calculated using the smooth particle-mesh Ewald method<sup>25,26</sup> with a real space cutoff of 12  $\text{\AA}$  and a reciprocal grid spacing of 1.2  $\text{\AA}$ . Lennard-Jones energies were cut off at 12  $\text{\AA}$ . A 2 fs time step was used and data collected every 5000 steps (10 ps).

The root-mean-square deviation (rmsd) from a reference structure, typically the initial structure, is the most commonly used measure to monitor structural changes over time; however, it is not the most suitable for the present case because applying pressure does not extensively deform the entire structure but distorts only the local structure around a central cleft, as illustrated in Figure 1. Instead of rmsd, here the time course of the distance between L8-C $\alpha$  and E34-C $\alpha$  ( $d_{\text{L8-E34}}$ ), which is also indicated in Figure 1, was followed to sensitively perceive the specific open-closed structural transition.

Water penetration into the protein interior was monitored in two ways, the number of “internal” water molecules ( $N_{\text{int-wat}}$ ) and the distance between the “cavity center” and the closest water molecule ( $d_{\text{cav-wat}}$ ).  $N_{\text{int-wat}}$  was defined according to Day and García<sup>10</sup> as follows. First, bulk water molecules were classified as water molecules that did not contact the protein. Then, water molecules that contacted the protein and did not contact the bulk water were defined as internal water molecules. A 3.5  $\text{\AA}$  distance cutoff between heavy atoms was used to define contacts. For calculation of  $d_{\text{cav-wat}}$ , the center of the internal cavity, where water molecules are expected to penetrate under high pressure,<sup>12</sup> was defined by the midpoint between L30-C $\alpha$  and L69-C $\alpha$ , as indicated in Figure 1.

The time course plots were smoothed with the sliding window width of 101 points for clear and distinct representation. The original plots are found in Supporting Information.

## Results and Discussion

**Protein Structural Transition.** Figure 2 shows the time courses of the ubiquitin structure monitored by  $d_{\text{L8-E34}}$  at 1, 3000, and 6000 bar. The measure exhibits a clear difference in the structure between low and high pressures. At pressures of 1 and 3000 bar,  $d_{\text{L8-E34}}$  fluctuates around small values of 9  $\text{\AA}$  for most of the time and occasionally becomes larger up to about 15  $\text{\AA}$ . In contrast, at 6000 bar it keeps large values around 15  $\text{\AA}$  for long periods and sometimes returns to small values. The trajectories imply that there are at least two stable conformations, one is a “closed” structure characterized with  $d_{\text{L8-E34}} \sim 9 \text{ \AA}$ ; the other is an “open” structure of  $d_{\text{L8-E34}} \sim 15 \text{ \AA}$ . The protein fluctuates between the closed and open conformational states on a time scale longer than 100 ns with high pressure shifting the equilibrium to the open state.

Figure 3 gives the probability density functions (PDFs) of  $d_{\text{L8-E34}}$  calculated from the trajectories. In fact, at least three distinct peaks that correspond to different protein structures are found in the PDFs. The distribution around 9  $\text{\AA}$  corresponds to the native structure under atmospheric pressure ( $N$ ), while that around 15  $\text{\AA}$  is a quasi-native structure stabilized under high pressure ( $N'$ ), which we expected to find. The distribution found between  $N$  and  $N'$  states can be regarded as an ensemble of transient metastable structures ( $N^*$ ). For more quantitative analysis, PDFs were decomposed into the three parts by

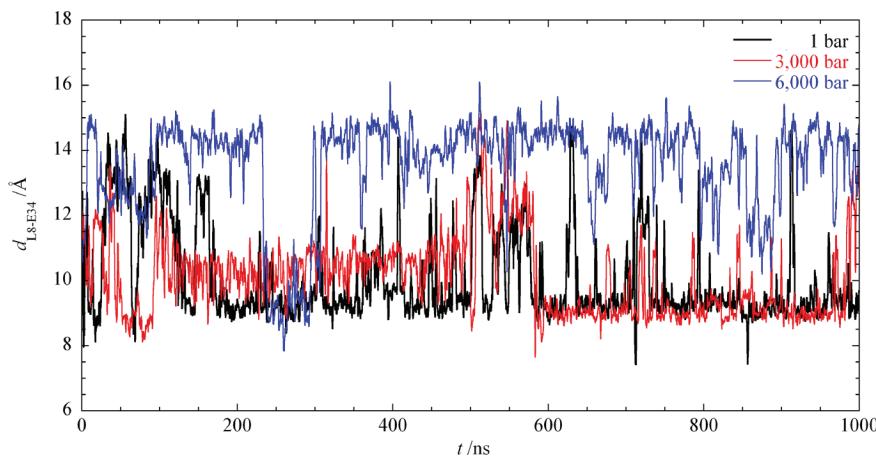


**Figure 2.** Smoothed plots of the time courses of the distance between the  $\alpha$ -carbons of L8 and E34 ( $d_{\text{L8-E34}}$ ) in the MD simulations at 1, 3000, and 6000 bar. The original plots are found in Supporting Information.

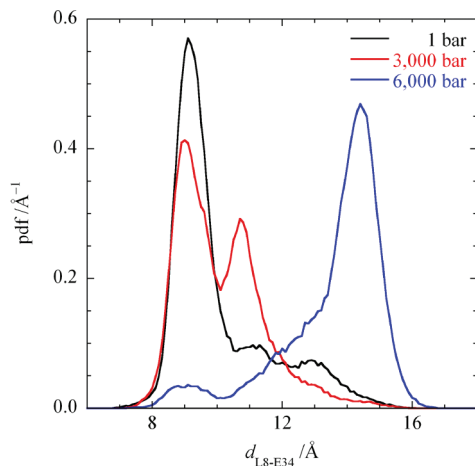


**Figure 3.** Probability density functions of the distance between the  $\alpha$ -carbons of L8 and E34 ( $d_{\text{L8-E34}}$ ) calculated from the MD trajectories at 1, 3000, and 6000 bar.

**TABLE 1: Content Percentages of Native ( $N$ ), Transient Metastable ( $N^*$ ), and High-Pressure Quasi-Native ( $N'$ ) Structures of Ubiquitin at Different Pressures**

	$N$	$N^*$	$N'$
1 bar	70%	30%	0%
3000 bar	53%	47%	0%
6000 bar	6%	28%	66%

Gaussian curve fitting, in which each of the  $N$  and  $N'$  distributions was fitted by a single Gaussian function and the  $N^*$  part given by a superposition of two or three Gaussian functions. Then, the content percentage was obtained by integrating the fitted curve. The results are given in Table 1. Obviously, the content of the  $N$  structure decreases with increasing pressure, although some still remains at 6,000 bar. In contrast, the content of the  $N'$  structure increases with increasing pressure. (The  $N'$  state is, though, apparently not observed at 1 and 3000 bar. It first appears at pressures between 3000 and 6000 bar).

These results lead to the following mechanism underlying the pressure-induced structural transition (Figure 4). The protein fluctuates between a few conformational states including the native state (in the present case,  $N$ ,  $N^*$ , and  $N'$ ) under equilibrium conditions at atmospheric pressure in a time scale of  $>100$  ns. Applying pressure shifts the equilibrium toward a conformational state with smaller PMV (in this case,  $N'$ ), rather than distorting the native structure itself or displacing the free energy minimum

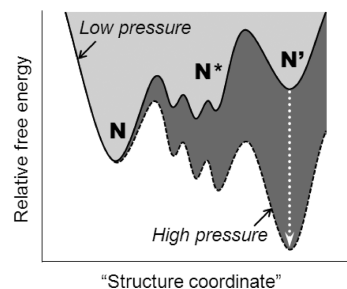


**Figure 4.** Schematic illustration of the change in the relative free energy profile due to applied pressure.  $N$ ,  $N^*$ , and  $N'$  denote the native, transient metastable, and high-pressure quasi-native structures, respectively.

of the native state. This molecular picture is qualitatively the same as that drawn from NMR observations.<sup>13,14</sup> In that study, they concluded that the protein exists in equilibrium between two major conformers  $N_1$  and  $N_2$ , in which  $N_1$  is dominant ( $\sim 85\%$ ) at 30 bar and  $N_2$  becomes more populated ( $\sim 77\%$ ) at 3000 bar. That is consistent with our result if we assume that  $N$  and  $N'$  correspond to  $N_1$  and  $N_2$ , respectively, and a part of  $N^*$  is assigned to  $N_1$  and the other part to  $N_2$  and that 3000 bar in the experiment reads 6000 bar in our simulation in a qualitative sense. We should emphasize that this picture was not obtained previously for short (several tens of nanoseconds) MD simulations.

**Water Penetration.** Figure 5a shows the time courses of water penetration represented by the number of the internal water molecules,  $N_{\text{int-wat}}$ , at the three pressures. On average, a larger number of water molecules penetrate into the protein interior as the pressure is increased. The time-averaged  $N_{\text{int-wat}}$  at 1, 3000, and 6000 bar are 17.9, 19.7, and 23.4, respectively. Our result is consistent with the change of  $N_{\text{int-wat}}$  from NMR-LPS at 1 bar ( $19 \pm 2$ ) to NMR-HPS at 6000 bar ( $25 \pm 2$ ) estimated by Day and García,<sup>10</sup> even though the same crystal structure is used as the initial structures in our three simulations under the different pressures. This coincidence allows us to conclude that our simulations succeed in the realization of a structural transition coupled with water penetration occurring under high pressure.

For the following quantitative analysis, we found that  $N_{\text{int-wat}}$  does not always accurately represent penetration of water into the specific cavity which is associated with a reduction in PMV of the protein.<sup>12</sup> Therefore, the distance between the cavity center and the closest water molecule,  $d_{\text{cav-wat}}$ , was monitored to investigate the specific water penetration. The results for the three pressures are given in Figure 5b. Obviously, water

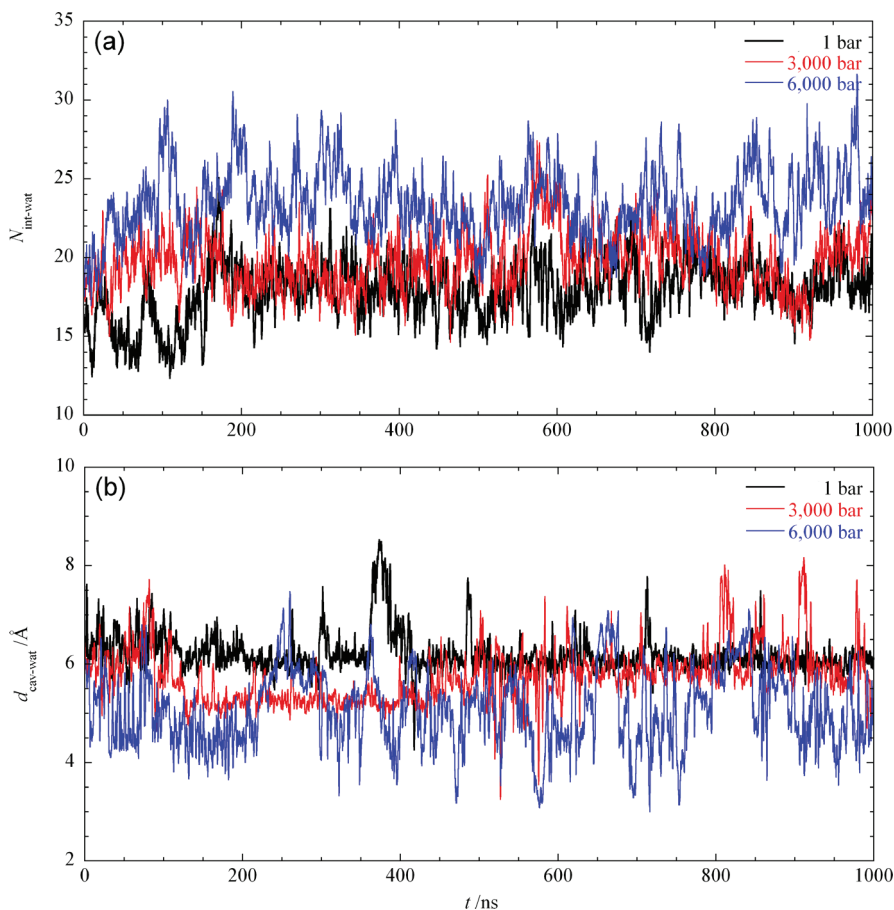


**Figure 5.** Smoothed plots of the time courses of water penetration in the MD simulations at 1, 3000, and 6000 bar. (a) The number of the internal water molecules ( $N_{\text{int-wat}}$ ). (b) The distance between the cavity center and the closest water molecule ( $d_{\text{cav-wat}}$ ). The original plots are found in Supporting Information.

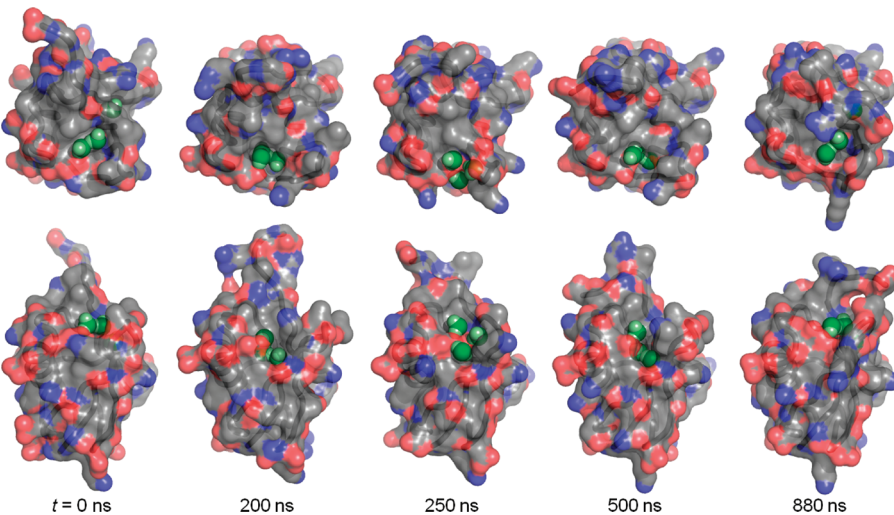


**Figure 6.** Top and side views of five representative snapshots from the MD trajectories at 6000 bar. The protein is represented by the translucent surface and tube model. Gray, red, and blue surfaces are of carbon, oxygen, and nitrogen, respectively. Hydrogens are not drawn. Only the first, second, and third closest water molecules to the cavity center are depicted as van der Waals spheres, where oxygen and hydrogen are colored green and pale green, respectively. In the second and fourth snapshot, the very closest water molecule is located deeper behind the two outer molecules. In the first and last snapshots, the third water molecule is found on the surface of the other side.

molecules reach even closer to the cavity as the pressure is elevated. Water molecules are frequently trying to approach the cavity at 6000 bar, whereas they maintain a distance of  $\sim 6$  Å from the cavity center over the simulation time at 1 bar.

**Dynamic Correlation between Protein Structural Transition and Water Penetration.** A comparison between Figures 2 and 5b shows a negative correlation between  $d_{\text{L8-E34}}$  and

$d_{\text{cav-wat}}$  at 6000 bar. The protein takes the open form (identified by a large value of  $d_{\text{L8-E34}}$ ) when water penetrates deeply into the protein ( $d_{\text{cav-wat}}$  becomes small), and vice versa. Figure 6 provides five representative snapshots from the MD trajectory at 6000 bar to illustrate this correlation. In the snapshots, only the first, second, and third closest water molecules to the cavity center are displayed. The cleft of the protein is closed at the

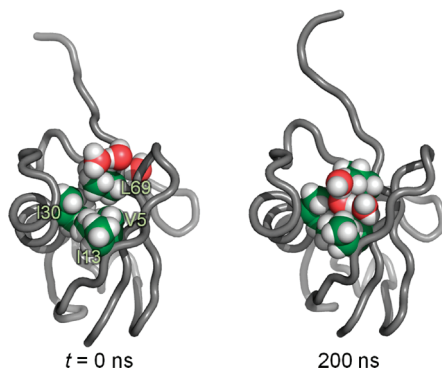


**Figure 7.** Structural change in the hydrophobic core composed of the V5, I13, I30, and L69 side chains associated with water penetration at 6000 bar. The side chain atoms are represented by van der Waals spheres, where carbon and hydrogen are colored green and white, respectively. Only the three closest water molecules are depicted as van der Waals spheres, where oxygen and hydrogen are colored red and white, respectively.

starting point ( $t = 0$  ns) and water molecules are merely located around the entrance, as shown in the first snapshot. Then, the cleft starts to fluctuate open and the protein maintains the open state roughly from 100 to 230 ns (see also Figure 2). During this period, a water molecule penetrates deeply into the open cleft (the second snapshot), where the innermost water molecule is buried among internal hydrophobic side chains of V5, I13, I30, and L69, while still keeping hydrogen bonds with the outer water molecules (see also Figure 7). The local structure created by the water penetration into the hydrophobic core resembles the water-mediated contact between methane molecules found by Hummer et al.<sup>7</sup> After this period, the cleft happens to close with the exclusion of water and the protein stays in the closed form for about 60 ns (the third snapshot). Then, the protein undergoes the second transition to the open form which also involves water penetration, followed by the long-time preservation of the open state until the end of the simulation (the fourth snapshot), though the protein sometimes shifts to the transient semiclosed state accompanying water exclusion (the last snapshot).

In order to quantify the dynamic correlation detected visually, we calculated the time cross-correlation function between  $d_{\text{L8-E34}}$  and  $d_{\text{cav-wat}}$ , defined by

$$C(t) = \frac{\langle \delta d_{\text{L8-E34}}(0) \delta d_{\text{cav-wat}}(t) \rangle}{\sqrt{\langle (\delta d_{\text{L8-E34}}(0))^2 \rangle} \sqrt{\langle (\delta d_{\text{cav-wat}})^2 \rangle}} \quad (1)$$

where brackets denote the time average over the simulation time and “ $\delta$ ” represents the deviation from the time average. As shown in Figure 8, the obtained correlation function exhibits a sharp negative peak at  $t = 0$ . This result signifies that the protein structural change and water penetration occurs simultaneously in the nanosecond time scale. When the peak is magnified up to 1000 times (see the inset of Figure 8), one can find both positive and negative time delays on the time scale of 10 ps. This time-lag is, however, most likely to be due to the dynamics of water itself, because it is comparable to the relaxation time of water.

The dynamic correlation found at 6000 bar is not observed at low pressures, especially at 1 bar. Although the protein occasionally exhibits opening motions even at 1 bar (See Figure 2), water molecules hardly come close to the cavity created by the opening motions (See Figure 5b).

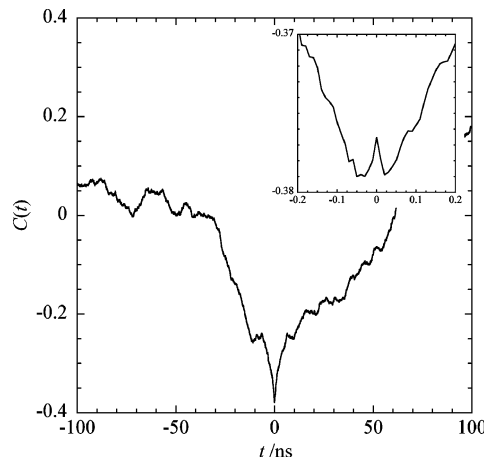


**Figure 8.** Time cross-correlation function between  $d_{\text{L8-E34}}$  and  $d_{\text{cav-wat}}$  for the simulation at 6000 bar. The inset shows a magnification around the peak at  $t = 0$  ns.

Thus, the simultaneous correlation between the protein structural change and water penetration is essential for steady stabilization of the open structure. The protein can fluctuate between the closed and open conformations irrespective of pressure. A transient open structure is maintained by the instantaneous penetration of water into the created cavity under high pressure, whereas it relaxes to the closed form without the water penetration under low pressure. This is a dynamic picture of the stabilization of HPS correlated with water penetration.

## Conclusions

In this study, the pressure-induced structural transition of ubiquitin, an opening of a central cleft, which has been observed by high-pressure NMR measurement, is successfully reproduced by 1  $\mu$ s MD simulations. The structural transition occurs under high pressure owing to the relative stabilization of a preexisting metastable structure rather than mechanical deformation of the native structure. The structural transition of the protein is accompanied by the penetration of water into the specific hydrophobic cleft within a time scale comparable to the relaxation time of water itself. Combining of the present results with those in a previous thermodynamic study,<sup>12</sup> one can conclude that water penetration is the primary driving force for protein denaturation under high pressure.

The content percentages of the conformers obtained in this study are rather qualitative because only a few conformational transitions were observed even in the microsecond-scale simulation and were statistically insufficient to determine quantitative values. In fact, the NMR study<sup>13</sup> estimated that the protein structure fluctuates in a time scale of tens of microseconds, implying that there is some slower process coupled with the structural transition and fluctuations found in this study. Generalized-ensemble methods such as replica-exchange MD<sup>27</sup> allow investigation of structural transitions more quantitatively from the viewpoint of statistics rather than dynamics. Work in this direction is in progress.

**Acknowledgment.** This work was supported by Research and Development of the Next-Generation Integrated Simulation of Living Matter, a part of the Development and Use of the Next-Generation Supercomputer Project of the Ministry of Education, Culture, Sports, Science, and Technology (MEXT), Japan. MD simulations were performed with the RIKEN Super Combined

Cluster (RSCC). T.I. thanks Yuka Torikoshi and Ryusuke Hiraoka who were involved in a preliminary study at Ritsumeikan University leading to the present work.

**Supporting Information Available:** Original plots for Figures 2 and 5. This material is available free of charge via the Internet at <http://pubs.acs.org>.

## References and Notes

- (1) Silva, J. L.; Weber, G. *Annu. Rev. Phys. Chem.* **1993**, *44*, 89.
- (2) Balny, C.; Masson, P.; Heremans, K. *Biochim. Biophys. Acta* **2002**, *1595*, 3.
- (3) Meersman, F.; Dobson, C. M.; Heremans, K. *Chem. Soc. Rev.* **2006**, *35*, 908.
- (4) Akasaka, K. *Chem. Rev.* **2006**, *106*, 1814.
- (5) Bridgman, P. W. *J. Biol. Chem.* **1914**, *19*, 511.
- (6) San Martín, M. F.; Barbosa-Cánovas, G. V.; Swanson, B. G. *Crit. Rev. Food Sci. Nutr.* **2002**, *42*, 627.
- (7) Hummer, G.; Garde, S.; García, A. E.; Paulaitis, M. E.; Pratt, L. R. *Proc. Natl. Acad. Sci. U.S.A.* **1998**, *95*, 1552.
- (8) Paliwal, A.; Asthagiri, D.; Bossev, D. P.; Paulaitis, M. E. *Biophys. J.* **2004**, *87*, 3479.
- (9) Collins, M. D.; Hummer, G.; Quillin, M. L.; Matthews, B. W.; Gruner, S. M. *Proc. Natl. Acad. Sci. U.S.A.* **2005**, *102*, 16668.
- (10) Day, R.; García, A. E. *Proteins: Struct., Funct., Bioinf.* **2008**, *70*, 1175.
- (11) Harano, Y.; Kinoshita, M. *J. Chem. Phys.* **2006**, *125*, 024910.
- (12) Imai, T.; Ohyama, S.; Kovalenko, A.; Hirata, F. *Protein Sci.* **2007**, *16*, 1927.
- (13) Kitahara, R.; Yokoyama, S.; Akasaka, K. *J. Mol. Biol.* **2005**, *347*, 277.
- (14) Kitahara, R.; Yamada, H.; Akasaka, K. *Biochemistry* **2001**, *40*, 13556.
- (15) Hess, B.; Kutzner, C.; van der Spoel, D.; Lindahl, E. *J. Chem. Theory Comput.* **2008**, *4*, 435.
- (16) Hornak, V.; Abel, R.; Okur, A.; Strockbine, B.; Boitberg, A.; Simmerling, C. *Proteins: Struct., Funct., Bioinf.* **2006**, *65*, 712.
- (17) Sorin, E. J.; Pande, V. S. *Biophys. J.* **2005**, *88*, 2472.
- (18) Vijay-Kumar, S.; Bugg, C. E.; Cook, W. J. *J. Mol. Biol.* **1987**, *194*, 531.
- (19) Berendsen, H. J. C.; Grigera, J. R.; Straatsma, T. P. *J. Phys. Chem.* **1987**, *91*, 6269.
- (20) Berendsen, H. J. C.; Postma, J. P. M.; DiNola, A.; Haak, J. R. *J. Chem. Phys.* **1984**, *81*, 3684.
- (21) Nosé, S. *Mol. Phys.* **1984**, *52*, 255.
- (22) Hoover, W. G. *Phys. Rev. A* **1985**, *31*, 1695.
- (23) Parrinello, M.; Rahman, A. *J. Appl. Phys.* **1981**, *52*, 7182.
- (24) Nosé, S.; Klein, M. L. *Mol. Phys.* **1983**, *50*, 1055.
- (25) Darden, T.; York, D.; Pedersen, L. *J. Chem. Phys.* **1993**, *98*, 10089.
- (26) Essmann, U.; Perera, L.; Berkowitz, M. L.; Darden, T.; Lee, H.; Pedersen, L. G. *J. Chem. Phys.* **1995**, *103*, 8577.
- (27) Sugita, Y.; Okamoto, Y. *Chem. Phys. Lett.* **1999**, *314*, 141.

JP909701J